journal of the mechanical behavior of biomedical materials 126 (2022) 105027

Contents lists available at ScienceDirect

Journal of the Mechanical Behavior of Biomedical Materials

journal homepage: www.elsevier.com/locate/jmbbm

Computational framework for analyzing flow-induced strain on osteocyte as modulated by microenvironment

Yoshitaka Kameo [a,b,c,*], Masahiro Ozasa [b], Taiji Adachi [a,b,c]

[a] Department of Biosystems Science, Institute for Frontier Life and Medical Sciences, Kyoto University, 53 Kawahara-cho, Shogoin, Sakyo-ku, Kyoto, 606-8507, Japan
[b] Department of Micro Engineering, Graduate School of Engineering, Kyoto University, 53 Kawahara-cho, Shogoin, Sakyo-ku, Kyoto, 606-8507, Japan
[c] Department of Mammalian Regulatory Network, Graduate School of Biostudies, Kyoto University, 53 Kawahara-cho, Shogoin, Sakyo-ku, Kyoto, 606-8507, Japan

ARTICLE INFO

Keywords:
Osteocyte
Canaliculus
Interstitial fluid flow
Mechanosensing
Fluid–structure interaction simulation

ABSTRACT

Osteocytes buried in bone matrix are major mechanosensory cells that regulate bone remodeling in response to interstitial fluid flow in a lacuno-canalicular porosity. To gain an understanding of the mechanism of osteocyte mechanosensing, it is important to be able to evaluate the local strain on the osteocyte process membrane induced by the interstitial fluid flow. The microenvironment of the osteocytes, including the pericellular matrix (PCM) and canalicular ultrastructure, is a key modulator of the flow-induced strain on the osteocyte process membrane because it produces heterogeneous flow patterns in the pericellular space. To investigate the effect of changes in the microenvironment of osteocytes on the flow-induced strain, we developed a novel computational framework for analyzing the fluid–structure interaction. Computer simulations based on the proposed framework enabled evaluation of the spatial distribution of flow-induced strain on the osteocyte process membrane according to changes in the PCM density and canalicular curvature. The simulation results reveal that a decrease in PCM density and an increase in canalicular curvature, each of which is associated with aging and bone disease, have the notable effect of enhancing local flow-induced strain on the osteocyte process membrane. We believe that the proposed computational framework is a promising framework for investigating cell-specific mechanical stimuli and that it has the potential to accelerate the mechanobiological study of osteocytes by providing a deeper understanding of their mechanical environment in living bone tissue.

1. Introduction

Osteocytes, the most abundant cell type in adult bone, are believed to function as mechanosensory cells (Bonewald, 2011). Their major role is to maintain the balance between osteoclastic bone resorption and osteoblastic bone formation corresponding to the given mechanical environment; hence, osteocytes are regarded as master regulators of bone remodeling. Osteocytes reside in lacuno-canalicular porosities within the mineralized bone matrix, forming an organized intercellular network interconnected by dendritic cell processes (Kamioka et al., 2009; Sugawara et al., 2011). Although such anatomical features cause the mechanical environment of osteocytes to be complex and unpredictable, it is widely accepted that the flow of interstitial fluid that fills the pericellular space in the lacuno-canalicular porosities plays an important role in osteocyte mechanosensing (Weinbaum et al., 1994).

In osteocyte mechanosensing, various membrane proteins acting as ion channels or cell adhesion molecules are responsible for converting flow-mediated mechanical forces into biochemical signals; this process is called mechanotransduction (Qin et al., 2020). The opening of mechanosensitive ion channels, such as Piezo1, caused by stretching of the osteocyte membrane, is a potent trigger of osteocyte mechanotransduction (Sasaki et al., 2020; Wang et al., 2020). Considering that the slender osteocyte processes are more sensitive to mechanical stimuli than are the osteocyte cell bodies (Adachi et al., 2009), evaluating the local strain on the osteocyte process membrane induced by interstitial fluid flow is highly important for gaining an understanding of the mechanism of osteocyte mechanosensing.

The local strain on the osteocyte process membrane is determined according to the fluid flow profile in the canaliculus, which is strongly modulated by the surrounding microenvironment. A pioneering study

Abbreviations: GAG, glycosaminoglycan; PCM, pericellular matrix; TE, tethering element; UHVEM, ultra-high-voltage electron microscope.

* Corresponding author. Mailing address: Department of Biosystems Science, Institute for Frontier Life and Medical Sciences, Kyoto University, 53 Kawahara-cho, Shogoin, Sakyo-ku, Kyoto, 606-8507, Japan.
E-mail address: kameo@infront.kyoto-u.ac.jp (Y. Kameo).

https://doi.org/10.1016/j.jmbbm.2021.105027
Received 14 September 2021; Received in revised form 19 November 2021; Accepted 2 December 2021
Available online 4 December 2021

by Weinbaum et al. (1994) showed that flow-induced shear stress acting on the osteocyte process membrane is a primary mechanical stimulus for the activation of osteocytes. A series of subsequent theoretical studies by their group proposed a possible mechanism of strain amplification on the osteocyte processes via the pericellular matrix (PCM), in which tethering elements (TEs) connecting the process to the canalicular wall play a critical role (Han et al., 2004; You et al., 2001). More specifically, it was shown that due to the fluid drag force, tensile force exerted by TEs on the osteocyte process membrane is much greater than the fluid shear force on the osteocyte process membrane. Furthermore, direct attachment of the osteocyte processes to canalicular projections via integrin-based focal adhesion has also been shown to contribute to the strain amplification (Vaughan et al., 2015; Wang et al., 2007). In conjunction with these connections between osteocyte processes and the canalicular wall, the complex structure of the lacuno-canalicular network, with its various curvatures, is another factor that can significantly affect the flow-induced strain on the osteocyte process membrane, owing to the production of heterogeneous flow patterns in the pericellular space (Anderson et al., 2005; Anderson and Tate, 2008; Kamioka et al., 2012).

For quantitatively evaluating the flow-induced strain on the osteocyte process membrane, computer simulation is a powerful tool. Finite element analysis using an osteocyte model reconstructed from confocal laser scanning images makes it possible to show the distribution of the surrounding fluid velocity and the flow-induced strain on the osteocytes (Verbruggen et al., 2012, 2014, 2016). However, confocal microscopy has insufficient resolution to visualize irregularities in the surface of the canalicular wall, such as canalicular projections. To capture the ultrastructure of osteocyte processes and the canalicular wall simultaneously, in our previous study, we constructed a three-dimensional model of osteocyte processes in canaliculi using ultra-high-voltage electron microscope (UHVEM) tomography (Kamioka et al., 2012). Simulation of the fluid–structure interaction using high-resolution UHVEM-image--based models has the potential to elucidate the manner in which the microenvironment of osteocytes influences local strain on the osteocyte process membrane (Yokoyama et al., 2021). For exploring the flow-induced strain on the osteocyte process membrane through such high-resolution fluid–structure interaction simulation, a computational framework that can consider both the PCM in canaliculi and the ultrastructure of osteocytes and/or canaliculi would be indispensable.

The aim of this study was to develop a computational framework for analyzing fluid–structure interaction to investigate the flow-induced strain on the osteocyte process membrane modulated by the microenvironment. The lattice Boltzmann method (Chen and Doolen, 1998) for fluid flow analysis and the finite element method for analyzing the deformation of the osteocyte process membrane were coupled using the immersed boundary method (Peskin, 2002). In this method, the effects of the PCM are represented by glycosaminoglycan (GAG), which influences the fluid pressure gradient in canaliculi, and TEs, which anchor the osteocyte processes to the canalicular wall as linear elastic springs. Considering that PCM density and the lacuno-canalicular structure are altered by aging and bone disease (Lai et al., 2015; Tiede-Lewis and Dallas, 2019; Wang et al., 2014), we investigated their effects on the spatial distribution of flow-induced strain on the osteocyte process membrane using the proposed framework together with three-dimensional models of a single canaliculus and an osteocyte process with idealized geometry.

2. Methods

2.1. Interstitial fluid flow in canaliculi

Interstitial fluid in a canaliculus flows through the PCM surrounding the osteocyte process; the PCM might consist of, for example, a proteoglycan comprising GAG and a core protein. For representing the flow in the pericellular space driven by the pressure gradient ∇p and body force $\boldsymbol{F}$, the fluid velocity $\boldsymbol{u}$ was assumed to be governed by the Brinkman equation:

$$\nabla p = -\frac{\mu}{k_\mathrm{p}}\boldsymbol{u} + \mu\nabla^2\boldsymbol{u} + \boldsymbol{F}, \tag{1}$$

where μ is the fluid viscosity, and k_p is the permeability of the PCM. The fluid flow governed by the Brinkman equation was numerically analyzed using the lattice Boltzmann method (Chen and Doolen, 1998). The D3Q19 model was used to discretize three-dimensional coordinate space and velocity space. The discretized lattice Boltzmann equation is given as follows:

$$f_i(\boldsymbol{x}+\boldsymbol{c}_i\Delta t, t+\Delta t) - f_i(\boldsymbol{x},t) = -\frac{1}{\tau}[f_i(\boldsymbol{x},t) - f_i^{\mathrm{eq}}(\boldsymbol{x},t)] + g_i\Delta t + h_i\Delta t + l_i\Delta t, \tag{2}$$

where $f_i(\boldsymbol{x}, t)$ is the particle distribution function with particle velocity $\boldsymbol{c}_i$ at position $\boldsymbol{x}$ and time t, Δt is the time step, and τ is the relaxation parameter. The equilibrium distribution function $f_i^{\mathrm{eq}}(\boldsymbol{x}, t)$ is expressed as

$$f_i^{\mathrm{eq}}(\boldsymbol{x},t) = \rho w_i\left[1 + \frac{\boldsymbol{c}_i\cdot\boldsymbol{u}}{c_\mathrm{s}^2} + \frac{(\boldsymbol{c}_i\cdot\boldsymbol{u})^2}{2c_\mathrm{s}^4} - \frac{\boldsymbol{u}\cdot\boldsymbol{u}}{2c_\mathrm{s}^2}\right], \tag{3}$$

where ρ is the fluid density, w_i is the weight, and c_s is the speed of sound defined in terms of the lattice interval Δx as $c_\mathrm{s} = \Delta x/(\sqrt{3}\,\Delta t)$. The kinematic viscosity of the fluid, ν, satisfies the following relationship:

$$\nu = \frac{\mu}{\rho} = \left(\tau - \frac{1}{2}\right)c_\mathrm{s}^2\Delta t. \tag{4}$$

In the last three terms on the right-hand side of Eq. (2), g_i, h_i, and l_i, which correspond to the body force, pressure gradient, and Darcy resistance, respectively, are given by

$$g_i = \left(1 - \frac{1}{2\tau}\right)w_i\left[\frac{\boldsymbol{c}_i - \boldsymbol{u}}{c_\mathrm{s}^2} + \frac{(\boldsymbol{c}_i\cdot\boldsymbol{u})\boldsymbol{c}_i}{c_\mathrm{s}^4}\right]\cdot\boldsymbol{F}, \tag{5}$$

$$h_i = \left(1 - \frac{1}{2\tau}\right)w_i\left[\frac{\boldsymbol{c}_i - \boldsymbol{u}}{c_\mathrm{s}^2} + \frac{(\boldsymbol{c}_i\cdot\boldsymbol{u})\boldsymbol{c}_i}{c_\mathrm{s}^4}\right]\cdot(-\nabla p), \tag{6}$$

$$l_i = \left(1 - \frac{1}{2\tau}\right)w_i\left[\frac{\boldsymbol{c}_i - \boldsymbol{u}}{c_\mathrm{s}^2} + \frac{(\boldsymbol{c}_i\cdot\boldsymbol{u})\boldsymbol{c}_i}{c_\mathrm{s}^4}\right]\cdot\left(-\frac{\mu}{k_\mathrm{p}}\boldsymbol{u}\right). \tag{7}$$

The macroscopic fluid density ρ and fluid velocity $\boldsymbol{u}$ are expressed using the particle distribution function, as follows:

$$\rho = \sum_i f_i, \tag{8}$$

$$\rho\boldsymbol{u} = \sum_i \boldsymbol{c}_i f_i + \frac{1}{2}\left(\boldsymbol{F} - \nabla p - \frac{\mu}{k_\mathrm{p}}\boldsymbol{u}\right)\Delta t. \tag{9}$$

2.2. Pressure gradient to drive fluid flow

The pressure gradient that drives interstitial fluid flow in canaliculi is induced by the application of mechanical load to the bone tissue. The fluid pressure gradient is expected to be altered by changes in the PCM permeability k_p, even under the same loading conditions. To estimate the fluid pressure gradient with respect to k_p, we utilized Biot's poroelastic theory (Biot, 1941, 1955). For the model of fluid-saturated bone tissue, we considered a single two-dimensional poroelastic trabecula with a width of $2a$ subjected to uniaxial cyclic loading $N(t) = N_0\sin 2\pi ft$, where N_0 is the amplitude per unit thickness, and f is the frequency (Kameo et al., 2008, 2009). In this model, the steady-state fluid pressure profile p_{steady} along the x axis (perpendicular to the loading direction) is given analytically in dimensionless form as

Table 1
Material properties and loading parameters of the trabecula for the poroelastic analysis. The fluid viscosity is from Cowin (1999), and the other material properties (shear modulus, drained Poisson's ratio, solid bulk modulus, fluid bulk modulus, and porosity) were determined by reference to Smit et al. (2002).

Symbol (unit)	Description	Value
μ (Pa·s)	Fluid viscosity	1.0×10^{-3}
G (GPa)	Shear modulus	5.94
ν	Drained Poisson's ratio	0.325
K_s (GPa)	Solid bulk modulus	17.66
K_f (GPa)	Fluid bulk modulus	2.3
φ	Porosity	0.01
a (μm)	Half-width of trabecula	100
N_0 (N/mm)	Amplitude of cyclic load	0.4
f (Hz)	Frequency of cyclic load	1

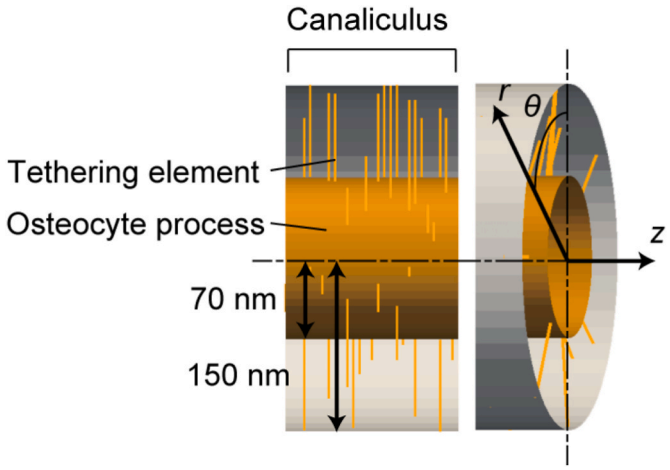

Fig. 1. Simulation model of a straight canaliculus and an osteocyte process.

$$p^*_{\text{steady}}(x^*, t^*) = \sin \Omega t^* - \text{Im}\left(\frac{H\sqrt{i\Omega}\cosh\sqrt{i\Omega}x^* - \sinh\sqrt{i\Omega}}{H\sqrt{i\Omega}\cosh\sqrt{i\Omega} - \sinh\sqrt{i\Omega}} e^{i\Omega t^*}\right), \tag{10}$$

where the superscript * indicates a dimensionless variable, and H and Ω are a dimensionless stress coefficient and dimensionless frequency, respectively (Kameo et al., 2009). Thus, the steady-state fluid pressure gradient is expressed as

$$\frac{\partial p^*_{\text{steady}}(x^*, t^*)}{\partial x^*} = -\text{Im}\left(\frac{iH\Omega \sinh\sqrt{i\Omega}x^*}{H\sqrt{i\Omega}\cosh\sqrt{i\Omega} - \sinh\sqrt{i\Omega}} e^{i\Omega t^*}\right). \tag{11}$$

We used the value of the amplitude of the fluid pressure gradient given in Eq. (11) at the trabecular surface ($x^* = \pm 1$) for the computational fluid dynamics analysis described in Section 2.1.

The dimensionless frequency Ω is defined using the permeability at the bone tissue scale, k (Kameo et al., 2008, 2009), and hence depends on the permeability at the PCM scale, k_p. By assuming isotropic orientation of the canaliculi, the bone tissue permeability k can be estimated from the following relationship (Kameo et al., 2010):

$$k = \frac{1}{3}\mu W \varphi, \tag{12}$$

where φ is the porosity of bone tissue, and W is a constant determined from the radius of the osteocyte process, r_p; the radius of the canaliculus, r_c; and k_p (Kameo et al., 2010). The PCM permeability k_p can be approximated as

$$k_p = 0.0572 a_0^2 \left(\frac{\Delta}{a_0}\right)^{2.377}, \tag{13}$$

where a_0 is the fiber radius, and Δ is the fiber spacing of the PCM (Tsay and Weinbaum, 1991). By setting a_0 and Δ according to the PCM alterations, we evaluated the fluid pressure gradient in canaliculi filled with PCM using Eqs. (11)–(13). The material properties of bone tissue modeled as a poroelastic material and the loading parameters are listed in Table 1 (Cowin, 1999; Smit et al., 2002).

2.3. Deformation of osteocyte process membrane

An osteocyte process inside a canaliculus was modeled as a deformable cylinder whose internal fluid is enclosed by a hyperelastic cell membrane. The two-dimensional membrane was assumed to follow the constitutive relation proposed by Skalak et al. (1973), the strain energy function of which is described as the following:

$$W = \frac{1}{4}G_s\left(I_1^2 + 2I_1 - 2I_2 + CI_2^2\right), \tag{14}$$

where G_s is the surface shear elastic modulus, and C is the area incompressibility coefficient associated with the ratio of the area dilation modulus to the shear elastic modulus, by which the surface Poisson's ratio is expressed as $\nu_s = C/(C+1)$. The variables I_1 and I_2 are the first and second strain invariants of the right Cauchy–Green tensor $\mathbf{C}$, given by

$$I_1 = \text{tr}\mathbf{C} - 2, \tag{15}$$

$$I_2 = \det\mathbf{C} - 1. \tag{16}$$

The membrane of the osteocyte process was discretized into flat triangular elements. The restoring force $\boldsymbol{q}_m$ due to the deformation of the membrane acting on the membrane node $\boldsymbol{x}_m$ was obtained using a finite element procedure.

A transverse tethering element (TE), which is regarded as a core protein of proteoglycan, was introduced as a linear elastic spring connecting a point $\boldsymbol{x}_m$ on the membrane of the osteocyte process to a point $\boldsymbol{x}_w$ on the canalicular wall. The restoring force $\boldsymbol{q}_t$ due to the stretching of the TE acting on the membrane node $\boldsymbol{x}_m$ can be described as

$$\boldsymbol{q}_t(\boldsymbol{x}_m) = \begin{cases} -k_t(|\boldsymbol{x}_m - \boldsymbol{x}_w| - L_0)\dfrac{\boldsymbol{x}_m - \boldsymbol{x}_w}{|\boldsymbol{x}_m - \boldsymbol{x}_w|} & \text{for } |\boldsymbol{x}_m - \boldsymbol{x}_w| > L_0 \\ \boldsymbol{0} \quad \text{for } |\boldsymbol{x}_m - \boldsymbol{x}_w| \le L_0 \end{cases}, \tag{17}$$

where k_t is the spring constant, and L_0 is the natural length of the TE. Thus, the total restoring force $\boldsymbol{q}$ acting on the membrane node $\boldsymbol{x}_m$ is given by

$$\boldsymbol{q}(\boldsymbol{x}_m) = \boldsymbol{q}_m(\boldsymbol{x}_m) + \boldsymbol{q}_t(\boldsymbol{x}_m). \tag{18}$$

2.4. Fluid–structure interaction analysis

The interstitial fluid flow and cell membrane deformation were coupled using the immersed boundary method (Peskin, 2002). In this method, the membrane force $\boldsymbol{q}$ is distributed to neighboring fluid nodes $\boldsymbol{x}_f$ and acts as an external body force $\boldsymbol{F}$ (Eq. (1)), which affects the fluid flow as follows:

$$\boldsymbol{F}(\boldsymbol{x}_f) = \sum D(\boldsymbol{x}_f - \boldsymbol{x}_m)\boldsymbol{q}(\boldsymbol{x}_m), \tag{19}$$

where $D(\boldsymbol{x})$ is the numerically approximated Dirac delta function given by

$$D(\boldsymbol{x}) = \begin{cases} \dfrac{1}{64\Delta x^3}\displaystyle\prod_{i=1}^{3}\left(1 + \cos\frac{\pi x_i}{2\Delta x}\right) & \text{for } |x_i| \le 2\Delta x,\ i = 1,\ 2,\ 3 \\ 0 \quad \text{otherwise} \end{cases}, \tag{20}$$

in which Δx is the lattice interval in the fluid domain (as in Section 2.1, where it also appears). The membrane velocity $\boldsymbol{U}$ is obtained by

Table 2
Material properties of the cell membrane and of the TEs for the fluid–structure interaction simulation. The membrane surface shear elastic modulus and area incompressibility coefficient were determined by reference to the elastic modulus of a mature osteocyte process in Sugawara et al. (2008).

Symbol (unit)	Description	Value
G_s (Pa·m)	Membrane surface shear elastic modulus	1.5×10^{-5}
C	Area incompressibility coefficient	10
k_t (N/m)	Spring constant of a tethering element	1.0×10^{-4}

interpolating the surrounding fluid velocity using the approximated Dirac delta function as follows:

$$\boldsymbol{U}(\boldsymbol{x}_m) = \sum D(\boldsymbol{x}_m - \boldsymbol{x}_f)\boldsymbol{u}(\boldsymbol{x}_f)\Delta x^3. \quad (21)$$

The cell membrane is advected with the velocity $\boldsymbol{U}$ by imposing a no-slip condition on the membrane surface.

2.5. Simulation models

2.5.1. Flow-induced strain on osteocytes modulated by pericellular matrix

Three-dimensional models of a single straight canaliculus and an osteocyte process for fluid–structure interaction simulation were constructed to evaluate flow-induced strain on the osteocyte process membrane (Fig. 1). The single canaliculus was regarded as a cylindrical tube having a length of 150 nm along the z axis. An osteocyte process with the same length as the canaliculus was modeled as a deformable cylinder covered with a hyperelastic membrane and placed coaxially inside the canalicular model. The radii of the canaliculus r_c and osteocyte process r_p were set to 150 nm and 70 nm, respectively (Lai et al., 2015).

The fluid-filled space in the canaliculus was discretized using a three-dimensional regular lattice with an interval Δx of 5 nm. This mesh size was sufficient to reproduce plug flow in the pericellular space, which was shown in the theoretical analysis (Weinbaum et al., 1994). To secure the same order of mesh size for analyzing the deformation of the osteocyte process membrane, the membrane was discretized using two-dimensional triangular elements with approximately 7 nm edge size. We confirmed that the finer discretization of the fluid-filled space and the osteocyte process membrane had negligible influence on the numerical results. To arrange TEs in the pericellular space, the attachment points of the TEs on the osteocyte process membrane were set randomly with respect to the central axis with a constant number density n. The other end of each TE was attached to the canalicular wall surface to align perpendicular to the osteocyte process membrane. The natural length L_0 of each TE, approximately 80 nm, was set as the length under no-flow condition which is equivalent to the interval of the pericellular space. We constructed 10 models with different TE configurations ($N = 10$) for each value of n.

Considering that the PCM density decreases as a result of aging and perlecan deficiency (Wang et al., 2014), we investigated the effects of decreases in GAG and TEs independently. The decrease in GAG was represented by an increase in PCM permeability k_p. Using a control value for k_p of 30 nm^2, we considered three conditions: $k_p = 30$, 60, and 120 nm^2. These values were estimated by substituting the physiological/pathological fiber radius a_0 and fiber spacing Δ (Wang et al., 2014) into Eq. (13). The corresponding fluid pressure gradients calculated from Eqs. (11) and (12) were $\partial p/\partial z = 64.8$ Pa/μm for $k_p = 30$ nm^2, $\partial p/\partial z = 34.7$ Pa/μm for $k_p = 60$ nm^2, and $\partial p/\partial z = 19.2$ Pa/μm for $k_p = 120$ nm^2. For the TEs, the decrease was represented by a decrease in their number density n, which indicates the number per unit length of the osteocyte process. Using a control value for n of 12/37.5 nm^{-1} (Wang et al., 2007), we considered three conditions: n = 12/37.5, 6/37.5, and 3/37.5 nm^{-1}. The other material properties of the cell membrane and TE used in the fluid–structure interaction simulation are listed in Table 2 (Sugawara et al., 2008).

As boundary conditions, the no-slip condition was applied at the canalicular wall, and the periodic boundary condition for the fluid velocity $\boldsymbol{u}$ and the membrane velocity $\boldsymbol{U}$ was applied at both ends of the canaliculus and the osteocyte process. A constant fluid pressure gradient along the z axis, $\partial p/\partial z$, with the values as given above, was imposed to drive the interstitial fluid flow in the canaliculus.

2.5.2. Flow-induced strain on osteocytes modulated by canalicular curvature

Osteocyte processes within canaliculi are reported to exhibit higher tortuosity in osteoporotic bone (Knothe Tate et al., 2004). Therefore, to investigate the effect of canalicular curvature on the flow-induced strain on the osteocyte process membrane, a three-dimensional model of a curved canaliculus containing a coaxial curved osteocyte process was constructed (Fig. 2). Two models of a single canaliculus and an osteocyte process with the same curvature radius R were smoothly connected. We

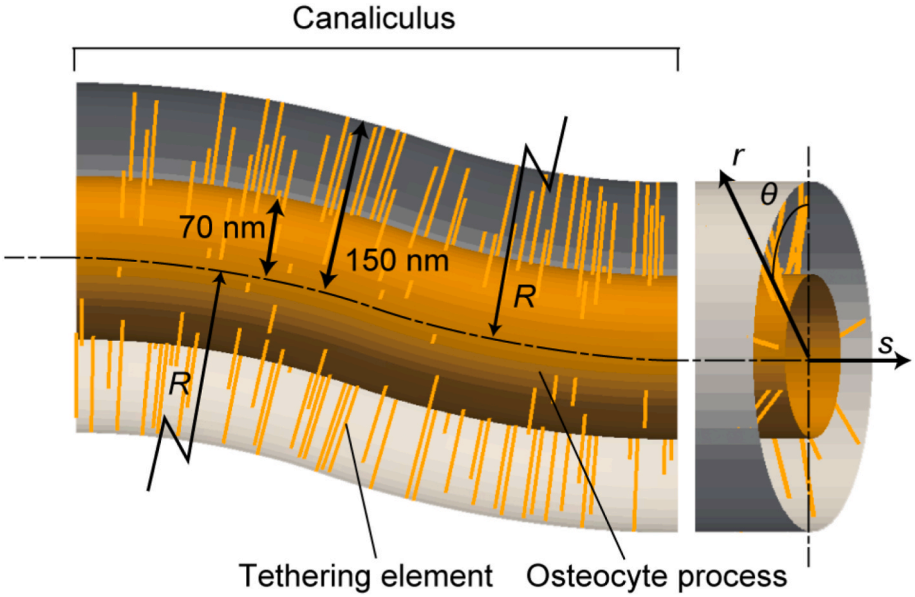

Fig. 2. Simulation model of a curved canaliculus and an osteocyte process.

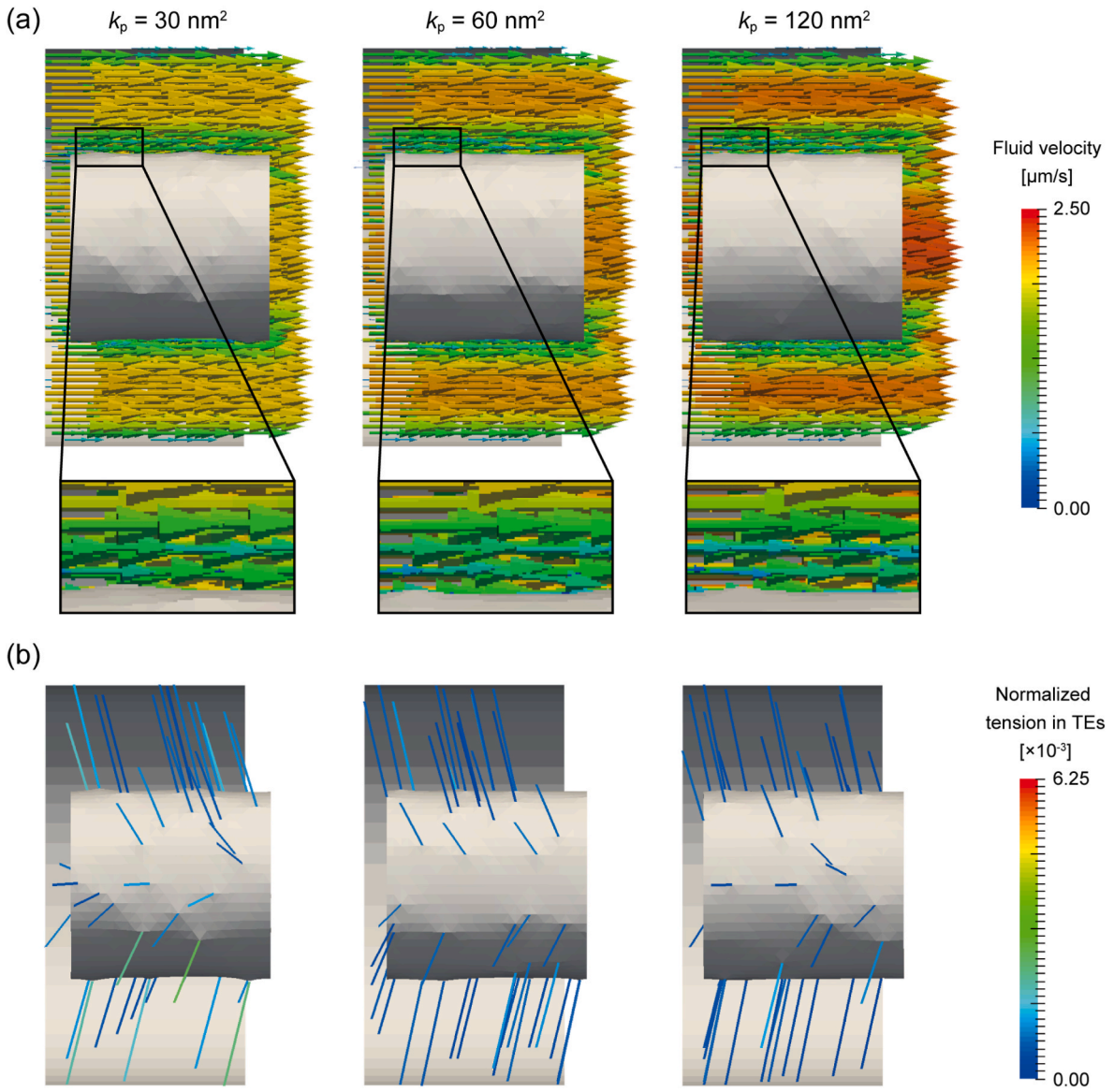

Fig. 3. Effect of a decrease in glycosaminoglycan (GAG), which is represented by an increase in pericellular matrix (PCM) permeability k_p, on the fluid velocity in the canaliculus and the tension in the tethering elements (TEs). (a) Distribution of the fluid velocity in the canaliculus when $k_p = 30, 60, 120$ nm^2. (b) Distribution of the tension in the TEs when $k_p = 30, 60, 120$ nm^2. The tension is normalized by $k_t L_0$.

considered three cases of curvature radii by reference to microscope images of bone specimens: $R = 1.2, 0.8, 0.4$ μm. A decrease in curvature radius corresponds to an increase in canalicular curvature. The total length of the simulation models along the central axis (the s direction) was set to 525 nm, regardless of R. The radii of the canaliculus, r_c, and of the osteocyte process, r_p, were set to 150 nm and 70 nm, respectively, the same as for the models described in Section 2.5.1.

The spatial discretization for the fluid-filled space in the canaliculus and the membrane of the osteocyte process were performed in common with that described in Section 2.5.1. The TEs aligned perpendicular to the osteocyte process membrane were arranged in the pericellular space according to the procedure shown in Section 2.5.1. The attachment points of the TEs on the osteocyte process membrane were randomly set with a number density of $n = 12/37.5$ nm^{-1}. We constructed 10 models with different TE configurations ($N = 10$). The PCM permeability k_p was set to 30 nm^2. The other material properties are listed in Table 2. The no-slip condition at the canalicular wall and the periodic boundary condition for the fluid velocity $\boldsymbol{u}$ and the membrane velocity $\boldsymbol{U}$ at both ends of the canaliculus and the osteocyte process were applied. A constant fluid pressure gradient along the central axis, $\partial p/\partial s = 64.8$ Pa/μm, was imposed to drive the interstitial fluid flow in the canaliculus.

All the simulations were performed using an in-house code written in CUDA C. The results were visualized using the open-source software ParaView (Kitware Inc.).

3. Results

3.1. Flow-induced strain on osteocytes modulated by pericellular matrix

3.1.1. Effect of glycosaminoglycan

We investigated the effect of GAG on the mechanical behavior of osteocyte processes by changing the PCM permeability ($k_p = 30$, 60, and 120 nm^2) under a constant number density of TEs ($n = 12/37.5$ nm^{-1}). A decrease in GAG, which is represented by an increase in k_p, enhanced the fluid velocity in the canaliculus because of the decrease in fluid resistance (Fig. 3a). However, it reduced the flow-induced shear force acting on the osteocyte process, resulting in a decrease in the tension in the supporting TEs (Fig. 3b). The spatial distribution of the flow-induced

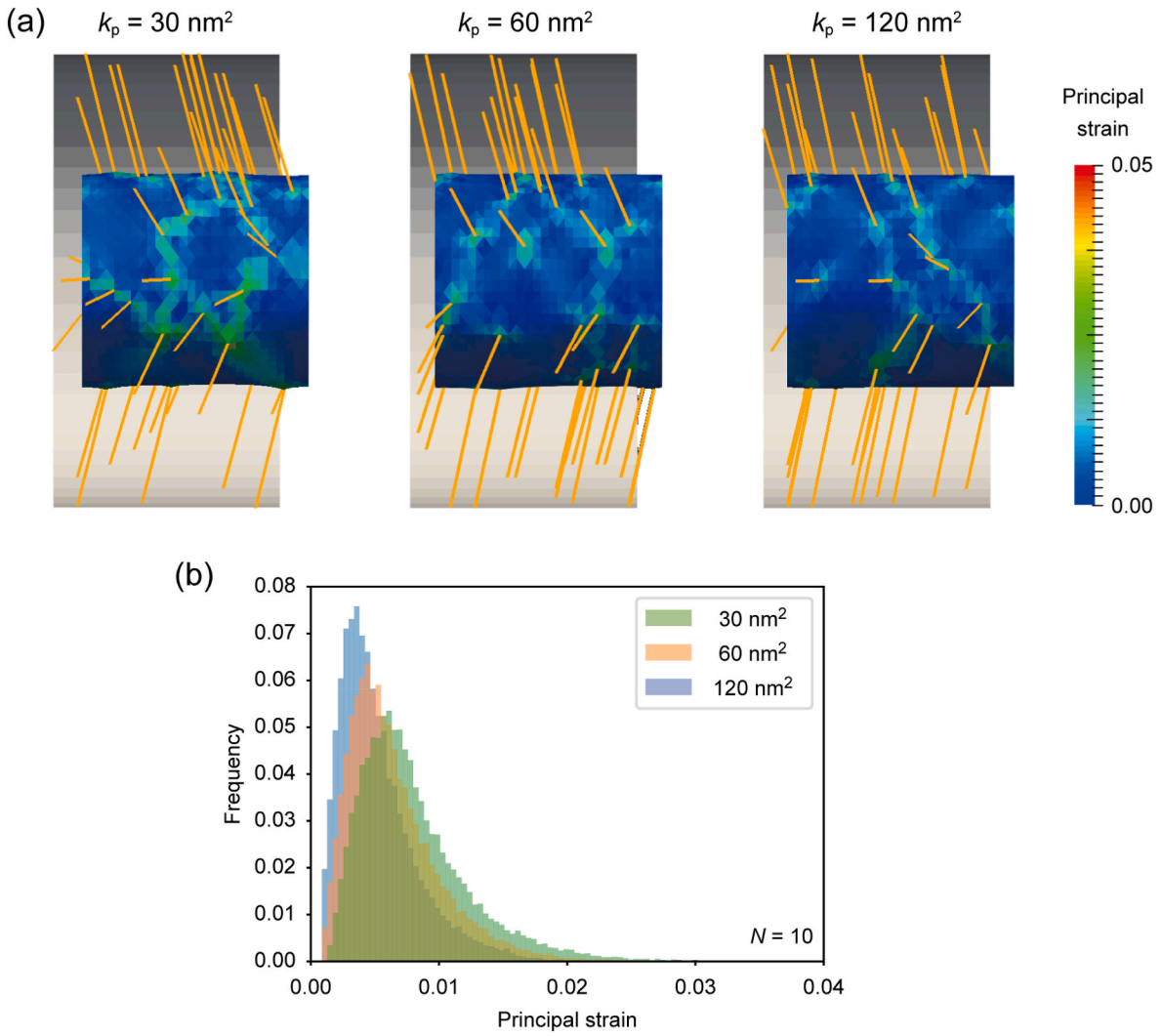

Fig. 4. Effect of a decrease in GAG, which is represented by an increase in PCM permeability k_p, on the flow-induced principal strain on the osteocyte process membrane. (a) Distribution of the principal strain on the osteocyte process membrane when k_p = 30, 60, 120 nm^2. (b) Histogram of the principal strain on the osteocyte process membrane for k_p = 30, 60, 120 nm^2 (N = 10 for each value of k_p).

strain on the osteocyte process membrane was closely related to that of the TEs (Fig. 4a). A high principal strain was observed in the neighborhood of the attachment regions of highly tensioned TEs. Thus, the decrease in GAG reduced osteocyte strain through a decrease in the tension in the TEs. For quantitative evaluation of the effect of GAG, the distribution of the principal strain is represented as a histogram (Fig. 4b). With a decrease in GAG, that is, an increase in k_p, both the mode and the variance of the principal strain decreased. These results show that a decrease in GAG can globally reduce the flow-induced strain on the osteocyte process membrane.

3.1.2. *Effect of tethering elements*

In parallel with the effect of GAG, we investigated the effect of another PCM constituent, TEs, on the mechanical behavior of osteocyte processes by changing their number density (n = 12/37.5, 6/37.5, and 3/37.5 nm^{-1}) under constant permeability (k_p = 30 nm^2). Because altering the number density of TEs does not affect the flow profile in the canaliculus (Fig. 5a), the flow-induced shear force acting on the osteocyte process remained constant. Therefore, decreasing the TEs increased the tension in each TE for supporting the osteocyte process subjected to a fluid shear force of unchanging magnitude (Fig. 5b). The highly tensioned TEs, which were observed when the number density of TEs was low, resulted in a strong concentration of the principal strain on the osteocyte process membrane (Fig. 6a). For quantitative evaluation of the effect of TEs, the distribution of the principal strain is represented as a histogram (Fig. 6b). Although the decrease in TEs had little influence on the general pattern of the histogram, it elongated the right tail. These results suggest that having a small number of TEs can produce a locally high strain on the osteocyte process membrane.

3.2. *Flow-induced strain on osteocytes modulated by canalicular curvature*

We investigated the effect of canalicular curvature on the interstitial fluid flow and on the flow-induced strain on the osteocyte process membrane. As the curvature radius R decreased, i.e., the curvature increased, the spatial distribution of fluid velocity in the canaliculus became more heterogeneous, leading to an increase in the maximum fluid velocity (Fig. 7a). The TEs located in the neighborhood of the inflection point of the canaliculus, where the fluid velocity changes markedly along the central axis, were particularly highly tensioned (Fig. 7b). When the canalicular curvature was relatively small (R = 1.2 μm), the regions of concentrated strain on the osteocyte process were randomly distributed (Fig. 8a). Meanwhile, a relatively large canalicular curvature (R = 0.4 μm) produced twin belt-like distributions of high principal strain on the osteocyte process membrane. The maximum

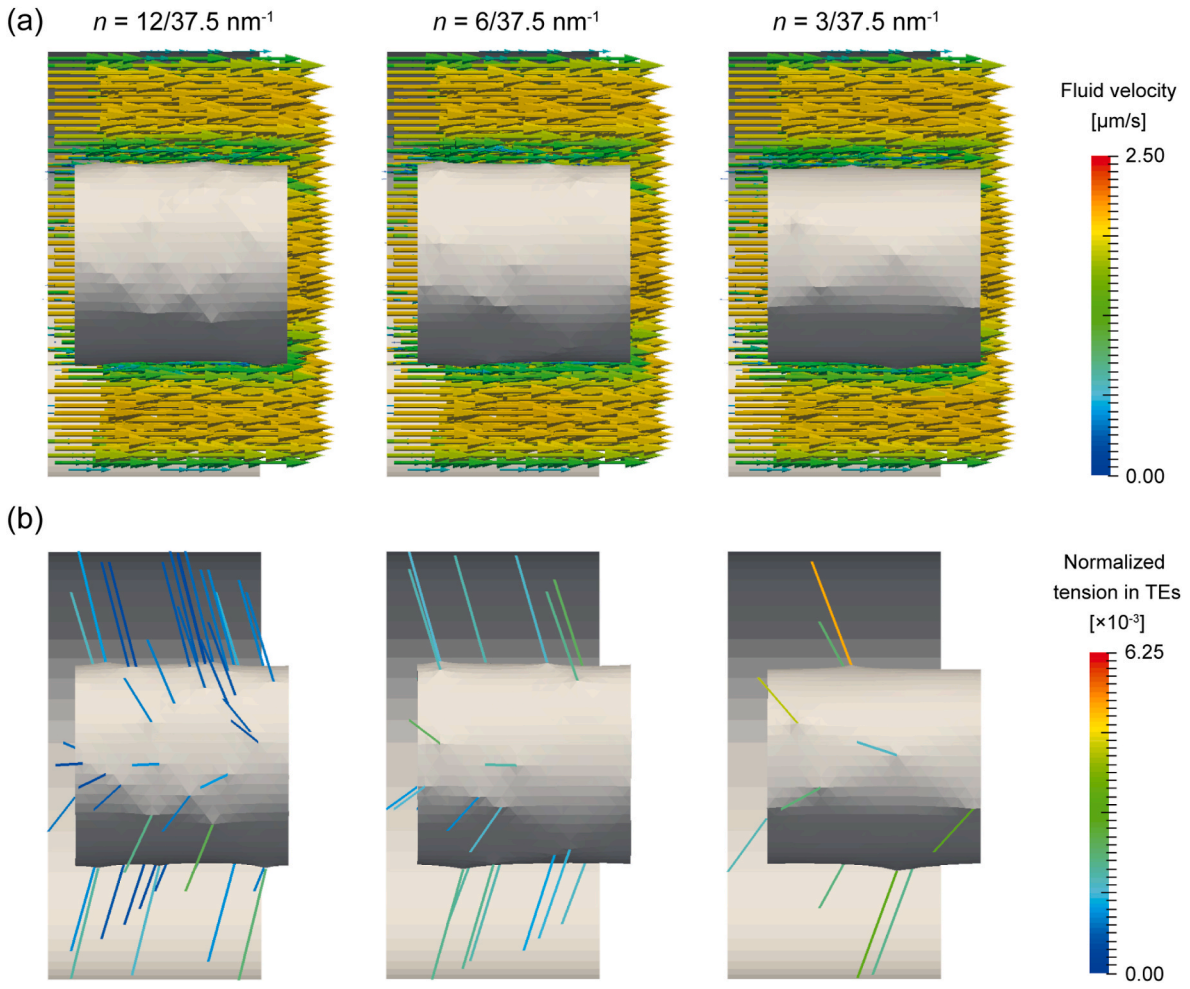

Fig. 5. Effect of a decrease in TEs, which is represented by a decrease in their number density n, on the fluid velocity in the canaliculus and the tension in the TEs. (a) Distribution of the fluid velocity in the canaliculus when n = 12/37.5, 6/37.5, 3/37.5 nm^{-1}. (b) Distribution of the tension in the TEs when n = 12/37.5, 6/37.5, 3/37.5 nm^{-1}. The tension is normalized by $k_t L_0$.

principal strain was observed in the region where the twin belts crossed, which coincides with the neighborhood of the inflection point of the canaliculus. This qualitative transition of the distribution of strain on the osteocyte process membrane associated with the increase in canalicular curvature is exhibited in the histogram of the principal strain as a marked elongation of the right tail (Fig. 8b). These results show that an increase in canalicular curvature can globally increase flow-induced strain on the osteocyte process membrane as well as dramatically changing its spatial distribution.

4. Discussion

We have developed a computational framework to investigate the effect of the microenvironment of osteocytes on the flow-induced strain on the osteocyte process membrane. This framework is novel in analyzing fluid–structure interaction that couples the interstitial fluid flow and the osteocyte process deformation and explicitly considers the effect of the PCM on the fluid flow dynamics in lacuno-canalicular porosity. Computer simulations using this framework enable the evaluation of the spatial distribution of flow-induced strain on the osteocyte process membrane, which can vary according to changes in its microenvironment, such as changes in PCM density and canalicular curvature. We anticipate that the proposed computational framework will contribute to the quantification of mechanical stimuli to osteocytes, which regulate bone remodeling, under physiological or pathological conditions.

Previous theoretical modeling studies suggested that the aspects of the osteocyte microenvironment, such as TEs and canalicular projections, can amplify local strain on the osteocyte process membrane (Han et al., 2004; Wang et al., 2007; You et al., 2001). Their approach, using an idealized cell-level model, elegantly highlights the essential strain amplification mechanism in osteocyte mechanosensing. However, these theoretical studies overlook the heterogeneity of the strain distribution on the osteocyte process membrane even though actual curved canaliculus produces heterogeneous flow patterns along the central axis direction, potentially enhancing local flow-induced strain on the osteocyte process membrane. The fluid–structure interaction simulation based on the present computational framework has revealed the concentration of strain on the osteocyte process membrane caused by the discrete arrangement of TEs in the pericellular space. Given that calcium transients in an osteocyte are induced by local deformation of its slender cell processes and subsequently propagate throughout the intracellular region (Adachi et al., 2009), locally high strain on the osteocyte process membrane could be a trigger of osteocyte mechanosensing. Hence, our computational framework, which enables quantitative evaluation of the local strain on the osteocyte process membrane, provides a powerful technique for understanding the molecular mechanism underlying osteocyte mechanosensing.

The interstitial fluid velocity surrounding osteocytes and the flow-induced strain on the osteocytes depend strongly on various factors such as mechanical loading condition of the bone tissue, location of the measuring osteocytes embedded in the bone tissue, and the condition of

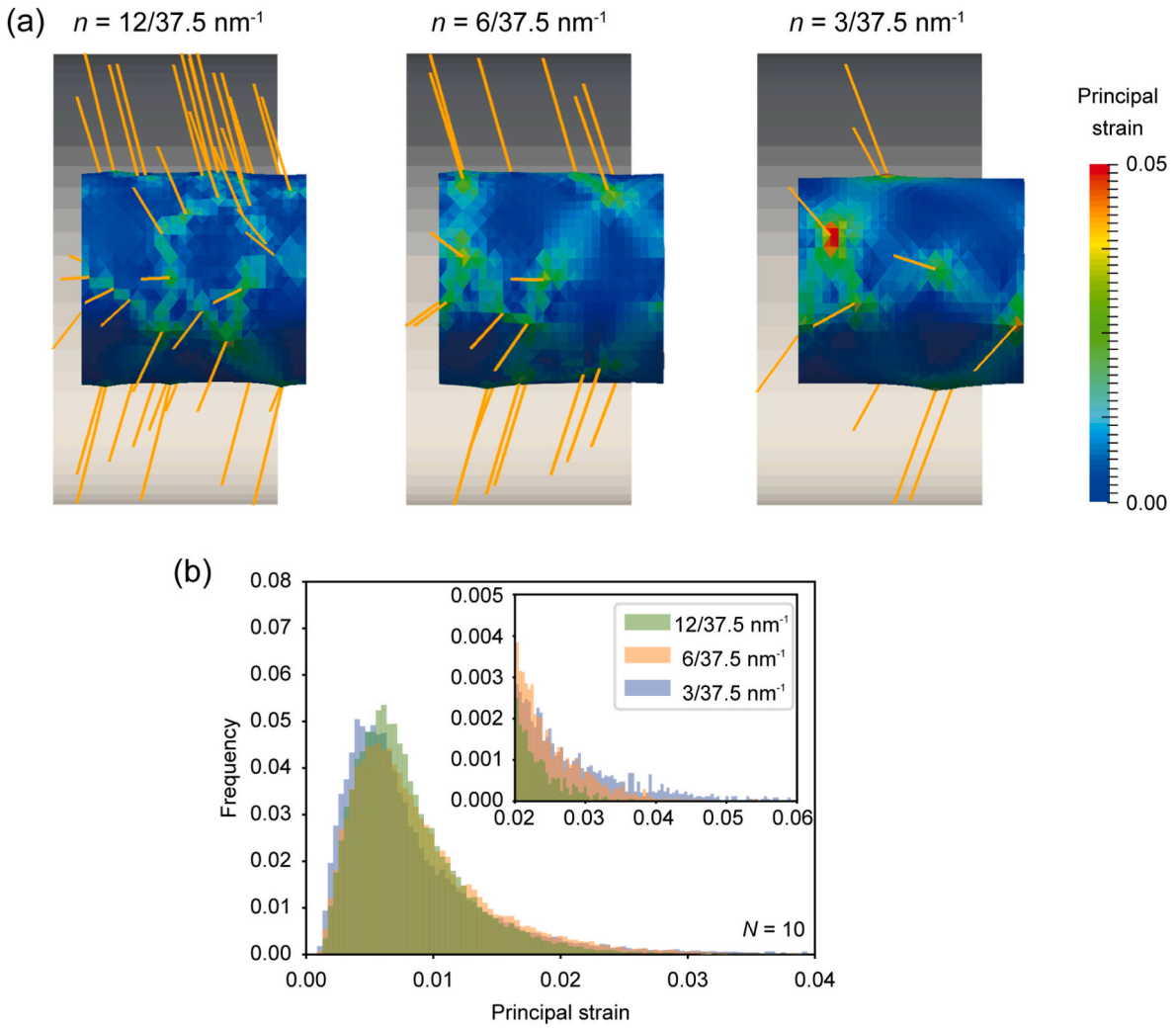

Fig. 6. Effect of a decrease in TEs, which is represented by a decrease in their number density n, on the flow-induced principal strain on the osteocyte process membrane. (a) Distribution of the principal strain on the osteocyte process membrane when n = 12/37.5, 6/37.5, 3/37.5 nm^{-1}. (b) Histogram of the principal strain on the osteocyte process membrane for n = 12/37.5, 6/37.5, 3/37.5 nm^{-1} (N = 10 for each value of n).

PCM. Therefore, it is difficult to quantitatively validate our simulation results through direct comparison with previous experimental findings. In the present study, we obtained approximately 2 μm/s fluid flow in canaliculi within a single trabecula subjected to cyclic loading with an amplitude of 2 MPa (or 127 με) and a frequency of 1 Hz. An experimental approach that combined fluorescence recovery after photobleaching technique and solute transport model of lacuno-canalicular system predicted the fluid velocity of 60 μm/s inside a cortical bone of mouse tibia under cyclic compression of 3 N peak load (or 400 με) at 0.5 Hz (Price et al., 2011). Considering the difference of mechanical loading conditions between these studies, our simulation results can be regarded as reasonable. We locally obtained over 10,000 με flow-induced strain on the osteocyte process membrane, which exceeded the strain level necessary for the mechano-response of bone cells in vitro (You et al., 2000). This strain level also coincides with the experimentally measured strain of osteocytes inside a cortical bone of rat femur under compressive loading of up to 3000 με at a strain rate of 83.3 με/s (Verbruggen et al., 2015).

The proposed computational framework allows investigating the effects of microenvironmental changes around osteocytes on their cellular mechanosensing, potentially including the roles of the integrin attachment of the osteocyte processes to canalicular projections and the complex structure of the lacuno-canalicular network. Although these important aspects have already been examined based on a fluid–structure interaction approach (Vaughan et al., 2015; Verbruggen et al., 2014, 2016), the PCM in canaliculi that can influence the fluid pressure gradient and the flow profile have not been considered, which may lead to misestimation of the flow-induced strain on the osteocyte process membrane. By modeling the PCM-dependent fluid pressure gradient and fluid flow, in the present study, we have successfully demonstrated the effect of PCM on the flow-induced mechanical stimuli to osteocytes. Osteocytic PCM density has been reported to decrease with aging and perlecan deficiency (Wang et al., 2014), implying that both GAG and TEs constituting the PCM can decrease under pathological conditions. Histological observations of the osteocyte network show that osteocyte processes exhibit higher tortuosity in osteoporotic bone (Knothe Tate et al., 2004), suggesting that the canalicular curvature is increased in bone diseases associated with aging. The present simulation results show that decreases in GAG and in TEs have opposite effects on the mechanical behavior of osteocyte processes: a decrease in GAG reduces the strain on the entire osteocyte process membrane, whereas a decrease in TEs produces strain concentrations near the existing TEs. Furthermore, an increase in canalicular curvature enhances the local strain on the osteocyte process membrane in the specific canalicular region. These results imply that the microenvironmental changes around osteocytes due to aging and bone disease have the effect of increasing local flow-induced strain on the osteocyte process membrane, which may be associated with bone pathologies. This increased

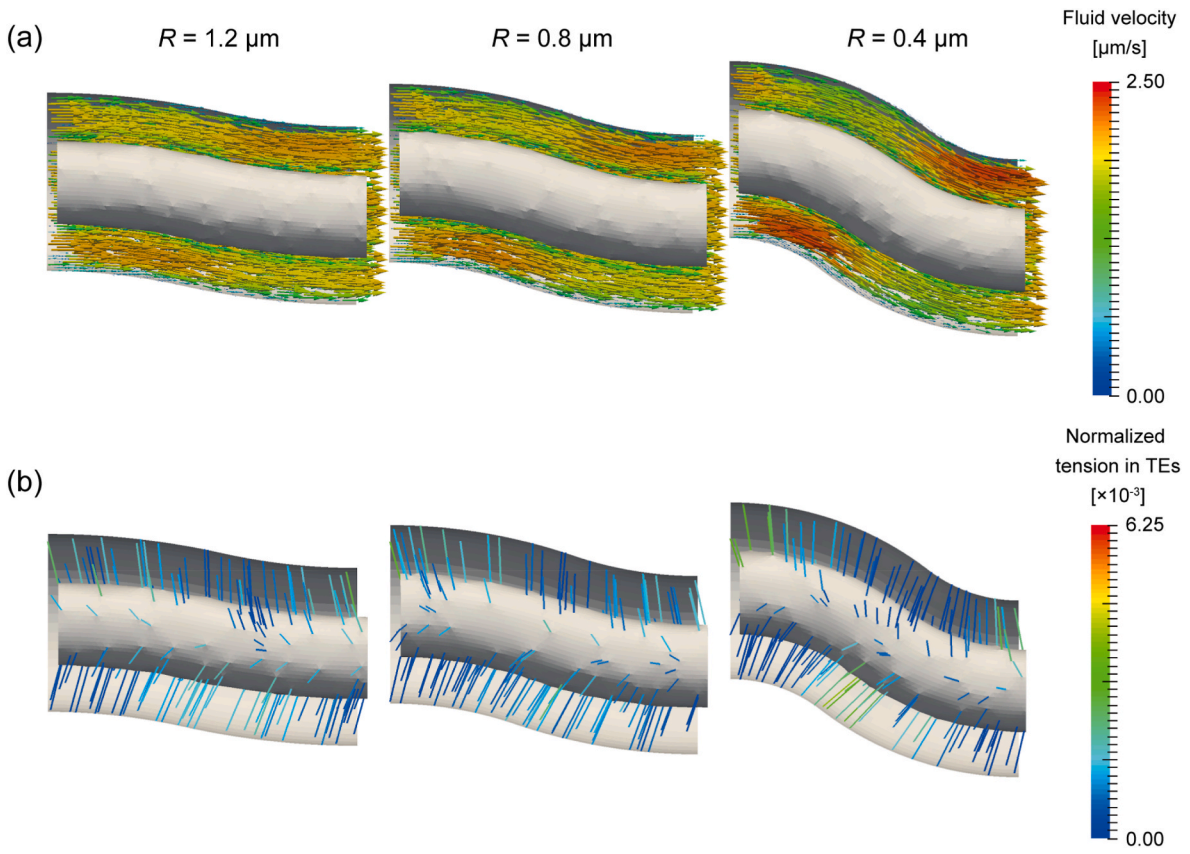

Fig. 7. Effect of an increase in canalicular curvature, which is represented by a decrease in its curvature radius R, on the fluid velocity in the canaliculus and the tension in the TEs. (a) Distribution of the fluid velocity in the canaliculus when $R = 1.2, 0.8, 0.4$ μm. (b) Distribution of the tension in the TEs when $R = 1.2, 0.8, 0.4$ μm. The tension is normalized by $k_t L_0$.

mechanical stimuli to osteocytes in aging and bone disease may be interpreted as a compensatory mechanism to maintain their mechanosensing even under low loading condition. Therefore, improving the conditions of the PCM and canaliculi around osteocytes may contribute to treating pathological bone states. There is a growing body of literature suggesting that osteocytes engage in resorbing and replacing local bone matrix, called as perilacunar/canalicular remodeling, to alter the lacuno-canalicular architecture (Bonewald, 2011; Yee et al., 2019). This can change the fluid flow dynamics in lacuno-canalicular porosity (Schurman et al., 2021), and may therapeutically regulate the mechanical stimuli to osteocytes.

One limitation of this study lies in the lack of incorporation of several intracellular structures that can play important roles in osteocyte mechanosensing, such as the cytoskeleton, integrin-based focal adhesion, and primary cilia, into the osteocyte process model (Qin et al., 2020). Osteocyte processes have distinct clusters of integrin $\alpha_v\beta_3$ binding intracellular cytoskeleton to extracellular bone matrix (Geoghegan et al., 2019), and direct attachment of the osteocyte processes to the canalicular wall via integrin-based focal adhesion is suggested to produce a membrane strain sufficiently high to open mechanosensitive ion channels (Vaughan et al., 2015; Wang et al., 2007). Although we avoided its modeling to maintain the canalicular shape as simple as possible, the most essential finding of these studies is that discrete attachments of osteocytes to the surrounding extracellular matrix, regardless of whether the attachment is via integrin or primary cilia, can produce locally high membrane strain. Thus, our claim that discretely arranged TEs have the notable effect of enhancing local flow-induced strain on the osteocyte process membrane is supported by the previous studies. A further extension of the simulation model by incorporating consideration of potential molecular mechanosensors would enable the analysis to identify the mechanical roles of each mechanosensor. An additional limitation is an insufficiency of experimentally measured data regarding PCM density and its dependency on aging and bone diseases. Although in this study we have shown the possible effects of the PCM, including GAG and TEs, on the mechanical behavior of osteocyte processes, future development of PCM measurement technology would improve the quantitative evaluation of the flow-induced strain on the osteocyte process membrane.

Despite the above limitations, the novel computational framework that we have proposed can quantify the local strain on the osteocyte process membrane, a trigger of osteocyte mechanosensing. This is a promising framework for investigating cell-specific mechanical stimuli using three-dimensional morphometric data for individual canaliculi and osteocyte processes (Yokoyama et al., 2021). We anticipate that this computational framework will accelerate the mechanobiological study of osteocytes through a deeper understanding of their mechanical environment in living bone tissue.

CRediT authorship contribution statement

Yoshitaka Kameo: Conceptualization, Methodology, Software, Writing - Original Draft, Writing - Review & Editing, Funding acquisition. **Masahiro Ozasa:** Software, Validation, Investigation, Visualization. **Taiji Adachi:** Conceptualization, Resources, Data Curation, Writing - Review & Editing, Supervision, Project administration, Funding acquisition.

Declaration of competing interest

The authors declare that they have no known competing financial interests or personal relationships that could have appeared to influence the work reported in this paper.

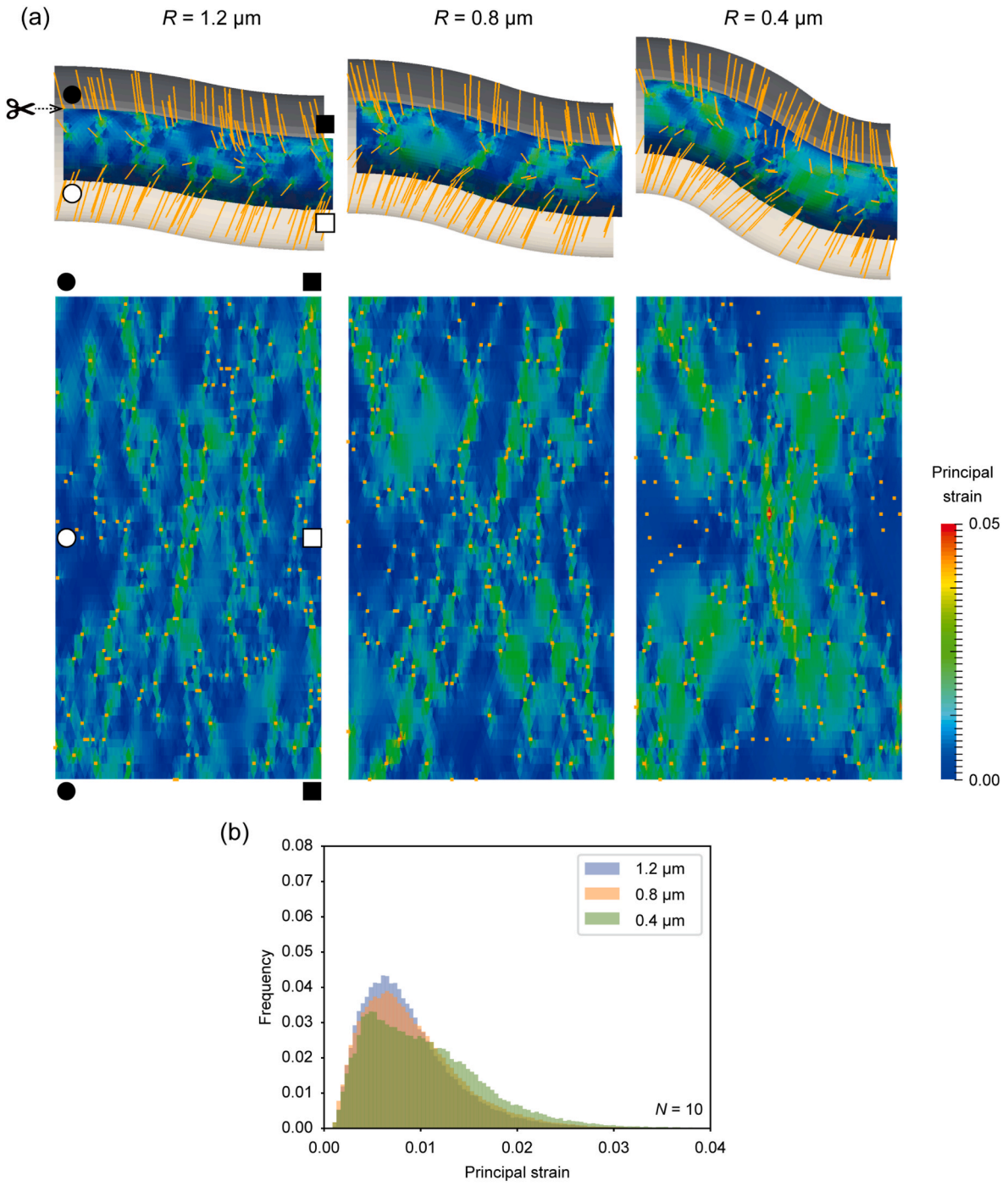

Fig. 8. Effect of an increase in canalicular curvature, which is represented by a decrease in its curvature radius R, on the flow-induced principal strain on the osteocyte process membrane. (a) Distribution of the principal strain on the osteocyte process membrane when $R = 1.2$, 0.8, 0.4 μm. Each osteocyte process is shown sliced open at the top; the horizontal axis is the s-coordinate and the vertical axis is the θ-coordinate. (b) Histogram of the principal strain on the osteocyte process membrane for $R = 1.2$, 0.8, 0.4 μm ($N = 10$ for each value of R).

Acknowledgments

This study was supported by the Japan Society for the Promotion of Science (JSPS) Grants-in-Aid for Scientific Research (C) (JP19K04074) and (A) (JP20H00659) and by the Japan Agency for Medical Research and Development (AMED) Advanced Research and Development Programs for Medical Innovation (AMED-CREST), Elucidation of Mechanobiological Mechanisms and Their Application to the Development of Innovative Medical Instruments and Technologies (JP20gm0810003).

References

Adachi, T., Aonuma, Y., Tanaka, M., Hojo, M., Takano-Yamamoto, T., Kamioka, H., 2009. Calcium response in single osteocytes to locally applied mechanical stimulus: differences in cell process and cell body. J. Biomech. 42, 1989–1995. https://doi.org/10.1016/j.jbiomech.2009.04.034.

Anderson, E.J., Kaliyamoorthy, S., Alexander, J.I.D., Tate, M.L.K., 2005. Nano-microscale models of periosteocytic flow show differences in stresses imparted to cell body and processes. Ann. Biomed. Eng. 33, 52–62. https://doi.org/10.1007/s10439-005-8962-y.

Anderson, E.J., Tate, M.L.K., 2008. Idealization of pericellular fluid space geometry and dimension results in a profound underprediction of nano-microscale stresses

imparted by fluid drag on osteocytes. J. Biomech. 41, 1736–1746. https://doi.org/10.1016/j.jbiomech.2008.02.035.
Biot, M.A., 1941. General theory of three-dimensional consolidation. J. Appl. Phys. 12, 155–164. https://doi.org/10.1063/1.1712886.
Biot, M.A., 1955. Theory of elasticity and consolidation for a porous anisotropic solid. J. Appl. Phys. 26, 182–185. https://doi.org/10.1063/1.1721956.
Bonewald, L.F., 2011. The amazing osteocyte. J. Bone Miner. Res. 26, 229–238. https://doi.org/10.1002/jbmr.320.
Chen, S., Doolen, G.D., 1998. Lattice Boltzmann method for fluid flows. Annu. Rev. Fluid Mech. 30, 329–364. https://doi.org/10.1146/annurev.fluid.30.1.329.
Cowin, S.C., 1999. Bone poroelasticity. J. Biomech. 32, 217–238. https://doi.org/10.1016/S0021-9290(98)00161-4.
Geoghegan, I.P., Hoey, D.A., McNamara, L.M., 2019. Integrins in osteocyte biology and mechanotransduction. Curr. Osteoporos. Rep. 17, 195–206. https://doi.org/10.1007/s11914-019-00520-2.
Han, Y.F., Cowin, S.C., Schaffler, M.B., Weinbaum, S., 2004. Mechanotransduction and strain amplification in osteocyte cell processes. Proc. Natl. Acad. Sci. U.S.A. 101, 16689–16694. https://doi.org/10.1073/pnas.0407429101.
Kameo, Y., Adachi, T., Hojo, M., 2008. Transient response of fluid pressure in a poroelastic material under uniaxial cyclic loading. J. Mech. Phys. Solid. 56, 1794–1805. https://doi.org/10.1016/j.jmps.2007.11.008.
Kameo, Y., Adachi, T., Hojo, M., 2009. Fluid pressure response in poroelastic materials subjected to cyclic loading. J. Mech. Phys. Solid. 57, 1815–1827. https://doi.org/10.1016/j.jmps.2009.08.002.
Kameo, Y., Adachi, T., Sato, N., Hojo, M., 2010. Estimation of bone permeability considering the morphology of lacuno-canalicular porosity. J. Mech. Behav. Biomed. Mater. 3, 240–248. https://doi.org/10.1016/j.jmbbm.2009.10.005.
Kamioka, H., Kameo, Y., Imai, Y., Bakker, A.D., Bacabac, R.G., Yamada, N., Takaoka, A., Yamashiro, T., Adachi, T., Klein-Nulend, J., 2012. Microscale fluid flow analysis in a human osteocyte canaliculus using a realistic high-resolution image-based three-dimensional model. Integr. Biol. 4, 1198–1206. https://doi.org/10.1039/c2ib20092a.
Kamioka, H., Murshid, S.A., Ishihara, Y., Kajimura, N., Hasegawa, T., Ando, R., Sugawara, Y., Yamashiro, T., Takaoka, A., Takano-Yamamoto, T., 2009. A method for observing silver-stained osteocytes in situ in 3-um sections using ultra-high voltage electron microscopy tomography. Microsc. Microanal. 15, 377–383. https://doi.org/10.1017/s1431927609990420.
Knothe Tate, M.L., Adamson, J.R., Tami, A.E., Bauer, T.W., 2004. The osteocyte. Int. J. Biochem. Cell Biol. 36, 1–8. https://doi.org/10.1016/s1357-2725(03)00241-3.
Lai, X.H., Price, C., Modla, S., Thompson, W.R., Caplan, J., Kirn-Safran, C.B., Wang, L.Y., 2015. The dependences of osteocyte network on bone compartment, age, and disease. Bone Res. 3 https://doi.org/10.1038/boneres.2015.9.
Peskin, C.S., 2002. The immersed boundary method. Acta Numer. 11, 479–517. https://doi.org/10.1017/S0962492902000077.
Price, C., Zhou, X., Li, W., Wang, L., 2011. Real-time measurement of solute transport within the lacunar-canalicular system of mechanically loaded bone: direct evidence for load-induced fluid flow. J. Bone Miner. Res. 26, 277–285. https://doi.org/10.1002/jbmr.211.
Qin, L., Liu, W., Cao, H.L., Xiao, G.Z., 2020. Molecular mechanosensors in osteocytes. Bone Res. 8 https://doi.org/10.1038/s41413-020-0099-y.
Sasaki, F., Hayashi, M., Mouri, Y., Nakamura, S., Adachi, T., Nakashima, T., 2020. Mechanotransduction via the Piezo1-Akt pathway underlies Sost suppression in osteocytes. Biochem. Biophys. Res. Commun. 521, 806–813. https://doi.org/10.1016/j.bbrc.2019.10.174.
Schurman, C.A., Verbruggen, S.W., Alliston, T., 2021. Disrupted osteocyte connectivity and pericellular fluid flow in bone with aging and defective TGF-beta signaling. Proc. Natl. Acad. Sci. U.S.A. 118 https://doi.org/10.1073/pnas.2023999118.
Skalak, R., Tozeren, A., Zarda, R.P., Chien, S., 1973. Strain energy function of red blood-cell membranes. Biophys. J. 13, 245–280. https://doi.org/10.1016/s0006-3495(73)85983-1.
Smit, T.H., Huyghe, J.M., Cowin, S.C., 2002. Estimation of the poroelastic parameters of cortical bone. J. Biomech. 35, 829–835. https://doi.org/10.1016/S0021-9290(02)00021-0.
Sugawara, Y., Ando, R., Kamioka, H., Ishihara, Y., Honjo, T., Kawanabe, N., Kurosaka, H., Takano-Yamamoto, T., Yamashiro, T., 2011. The three-dimensional morphometry and cell-cell communication of the osteocyte network in chick and mouse embryonic calvaria. Calcif. Tissue Int. 88, 416–424. https://doi.org/10.1007/s00223-011-9471-7.
Sugawara, Y., Ando, R., Kamioka, H., Ishihara, Y., Murshid, S.A., Hashimoto, K., Kataoka, N., Tsujioka, K., Kajiya, F., Yamashiro, T., Takano-Yarnamoto, T., 2008. The alteration of a mechanical property of bone cells during the process of changing from osteoblasts to osteocytes. Bone 43, 19–24. https://doi.org/10.1016/j.bone.2008.02.020.
Tiede-Lewis, L.M., Dallas, S.L., 2019. Changes in the osteocyte lacunocanalicular network with aging. Bone 122, 101–113. https://doi.org/10.1016/j.bone.2019.01.025.
Tsay, R.Y., Weinbaum, S., 1991. Viscous flow in a channel with periodic cross-bridging fibers - exact solutions and brinkman approximation. J. Fluid Mech. 226, 125–148. https://doi.org/10.1017/S0022112091002318.
Vaughan, T.J., Mullen, C.A., Verbruggen, S.W., McNamara, L.M., 2015. Bone cell mechanosensation of fluid flow stimulation: a fluid-structure interaction model characterising the role integrin attachments and primary cilia. Biomech. Model. Mechanobiol. 14, 703–718. https://doi.org/10.1007/s10237-014-0631-3.
Verbruggen, S.W., Mc Garrigle, M.J., Haugh, M.G., Voisin, M.C., McNamara, L.M., 2015. Altered mechanical environment of bone cells in an animal model of short- and long-term osteoporosis. Biophys. J. 108, 1587–1598. https://doi.org/10.1016/j.bpj.2015.02.031.
Verbruggen, S.W., Vaughan, T.J., McNamara, L.M., 2012. Strain amplification in bone mechanobiology: a computational investigation of the in vivo mechanics of osteocytes. J. R. Soc. Interface 9, 2735–2744. https://doi.org/10.1098/rsif.2012.0286.
Verbruggen, S.W., Vaughan, T.J., McNamara, L.M., 2014. Fluid flow in the osteocyte mechanical environment: a fluid-structure interaction approach. Biomech. Model. Mechanobiol. 13, 85–97. https://doi.org/10.1007/s10237-013-0487-y.
Verbruggen, S.W., Vaughan, T.J., McNamara, L.M., 2016. Mechanisms of osteocyte stimulation in osteoporosis. J. Mech. Behav. Biomed. Mater. 62, 158–168. https://doi.org/10.1016/j.jmbbm.2016.05.004.
Wang, B., Lai, X.H., Price, C., Thompson, W.R., Li, W., Quabili, T.R., Tseng, W.J., Liu, X. S., Zhang, H., Pan, J., Kirn-Safran, C.B., Farach-Carson, M.C., Wang, L.Y., 2014. Perlecan-containing pericellular matrix regulates solute transport and mechanosensing within the osteocyte lacunar-canalicular system. J. Bone Miner. Res. 29, 878–891. https://doi.org/10.1002/jbmr.2105.
Wang, L.J., You, X.L., Lotinun, S., Zhang, L.L., Wu, N., Zou, W.G., 2020. Mechanical sensing protein PIEZO1 regulates bone homeostasis via osteoblast-osteoclast crosstalk. Nat. Commun. 11 https://doi.org/10.1038/s41467-019-14146-6.
Wang, Y., McNamara, L.M., Schaffler, M.B., Weinbaum, S., 2007. A model for the role of integrins in flow induced mechanotransduction in osteocytes. Proc. Natl. Acad. Sci. U.S.A. 104, 15941–15946. https://doi.org/10.1073/pnas.0707246104.
Weinbaum, S., Cowin, S.C., Zeng, Y., 1994. A model for the excitation of osteocytes by mechanical loading-induced bone fluid shear stresses. J. Biomech. 27, 339–360. https://doi.org/10.1016/0021-9290(94)90010-8.
Yee, C.S., Schurman, C.A., White, C.R., Alliston, T., 2019. Investigating osteocytic perilacunar/canalicular remodeling. Curr. Osteoporos. Rep. 17, 157–168. https://doi.org/10.1007/s11914-019-00514-0.
Yokoyama, Y., Kameo, Y., Kamioka, H., Adachi, T., 2021. Image-based simulation reveals membrane strain concentration on osteocyte processes caused by tethering elements. Biomech. Model. Mechanobiol. 20, 2353–2360. https://doi.org/10.1007/s10237-021-01511-y.
You, J., Yellowley, C.E., Donahue, H.J., Zhang, Y., Chen, Q., Jacobs, C.R., 2000. Substrate deformation levels associated with routine physical activity are less stimulatory to bone cells relative to loading-induced oscillatory fluid flow. J. Biomech. Eng. 122, 387–393. https://doi.org/10.1115/1.1287161.
You, L., Cowin, S.C., Schaffler, M.B., Weinbaum, S., 2001. A model for strain amplification in the actin cytoskeleton of osteocytes due to fluid drag on pericellular matrix. J. Biomech. 34, 1375–1386. https://doi.org/10.1016/S0021-9290(01)00107-5.